Polymers **2015**, *7*, 1660-1673; doi:10.3390/polym7091476

OPEN ACCESS

polymers

ISSN 2073-4360

www.mdpi.com/journal/polymers

Article

Preparation and Characterization of Mn/N Co-Doped TiO_2 Loaded on Wood-Based Activated Carbon Fiber and Its Visible Light Photodegradation

Xiaojun Ma * and Yin Chen

Department of Wood Science and Technology, Tianjin University of Science & Technology, Tianjin 300222, China; E-Mail: chenyin@tust.edu.cn

* Author to whom correspondence should be addressed; E-Mail: mxj75@tust.edu.cn; Tel.: +86-22-6027-4494; Fax: +86-22-6027-3395.

Academic Editor: Michael K. C. Tam

Received: 18 June 2015 / Accepted: 27 August 2015 / Published: 7 September 2015

Abstract: Using $MnSO_4 \cdot H_2O$ as manganese source and urea as nitrogen source, Mn/N co-doped TiO_2 loaded on wood-based activated carbon fiber (Mn/Ti-N-WACF) was prepared by sol–gel method. Mn/Ti-N-WACF with different Mn doping contents was characterized by scanning electron microscopy, X-ray diffraction (XRD) and X-ray photoelectron spectroscopies (XPS), and ultraviolet-visible spectrophotometer. Results showed that the loading rate of TiO_2 in Mn/Ti-N-WACF was improved by Mn/N co-doping. After calcination at 450 °C, the degree of crystallinity of TiO_2 was reduced due to Mn/N co-doption in the resulting Mn/Ti-N-WACF samples, but the TiO_2 crystal phase was not changed. XPS spectra revealed that some Ti^{4+} ions from the TiO_2 lattice of Mn/Ti-N-WACF system were substituted by doped Mn. Moreover, new bonds formed within N–Ti–N and Ti–N–O because of the doped N that substituted some oxygen atoms in the TiO_2 lattice. Notably, the degradation rate of methylene blue for Mn/Ti-N-WACF was improved because of the co-doped Mn/N under visible-light irradiation.

Keywords: wood-based activated carbon fiber; Mn/N co-doped TiO_2; surface functional group; photodegradation

1. Introduction

TiO_2 is a commonly known semiconductor with photocatalytic activities that are attracting extensive interest because of its special optoelectronic and physiochemical properties [1]. It could potentially be used in various applications, including wastewater treatment, air purification, disinfection, and surface self-cleaning [2,3]. However, its low utilization ability of visible light and secondary pollution have limited its applications in some areas. In brief, the bandgap width of anatase TiO_2 is 3.2 eV, and its excitation wavelength is 387 nm. Thus, only the part of ultraviolet (UV) light with wavelength <387 nm can excite the photocatalytic activity of TiO_2, while, >90% of visible light cannot be utilized [4–6]. On the other hand, the separation of the fine TiO_2 powder from solution after degradation is challenging and costly [7–9]. Considerable efforts have been devoted to preparing visible-light-active TiO_2 materials and support materials with larger adsorption capacities in order to utilize TiO_2 more effectively.

To increase the visible light absorption of TiO_2 materials, transition metals were added into TiO_2 to improve its photocatalytic activity by reducing the energy bandgap width or preventing (e^-/h*) pair recombination through electron/hole trapping [10–18]. However, it was well-known that the transition metals doped TiO_2 suffered from the poor stability for the long-term operation. More recently, numerous studies have been focused on preparing N-doped TiO_2 powders and films via various synthesis routes [19,20]. It was proved that after N atom was doped into the TiO_2 anatase lattice a donor state was formed just above the valence band, which enhances its visible light absorbance. Other researchers found that transition metals/N co-doped into TiO_2 would facilitate the development of photocatalysts [21–23]. In addition, activated carbon fibers (ACFs) showing good adsorption and uniform pore structure have been used as catalyst supports for TiO_2 loading. However, ACFs, as a good choice of supporting material, are mainly prepared from fossil resources [24,25], which are considered to have a negative effect in terms of sustainability. Our group has previously reported the production of ACFs from renewable resources (woody biomass) (WACF) as support for TiO_2 loading [26,27].

In the present work, WACF composite loaded with Mn/N-co-doped TiO_2 (Mn/Ti-N-WACF) was prepared by sol–gel and impregnation method. The influences of Mn doping contents on the structure, surface groups, and visible light absorption of Mn/Ti-N-WACF were investigated using scanning electron microscopy, X-ray photoelectron spectroscopy, and ultraviolet–visible (UV-vis) spectrophotometer, respectively. In addition, the photocatalytic degradation behavior of methylene blue (MB) was used to evaluate the photoactivities of the prepared samples.

2. Experimental Section

2.1. Samples

A series of Mn/N co-doped TiO_2 with different Mn doping contents was prepared using sol–gel method. In a typical procedure, 0.03 mol of tetrabutyl orthotitanate ($C_{16}H_{36}O_4Ti$, Damao Chemical Reagent Factory, Tianjin, China) was dissolved in 60 mL of ethanol, a certain amount of $MnSO_4$ solution was then added with molar ratio of Mn:Ti from 0 to 2%. The solution was stirred for 30 min until it became completely transparent. Meanwhile, 2 mL of acetic acid was added to 60 mL of ethanol and 2.2 mL of the distilled water to from another solution. The latter solution and 0.3 g of urea were slowly added to the former one under vigorous stirring until completely dissolved. Finally, the mixed solution

was placed in a thermostatic water bath at 40 °C for 2 h for aging to obtain a milky white colloidal solution consisting of Mn/N co-doped TiO_2 sol.

Previously characterized WACF samples [28] were added into the above solution and mixed by vibration for 30 min. After a certain time of still dipping, the fibers were dried at 105 °C for 2 h, followed by the calcination at 450 °C for 1.5 h under a dry flow of air and then cooled to room temperature. The weight of the Mn/Ti-N-WACF photocatalytic material was recorded. The samples prepared from different Mn:Ti molar ratios: 0:1, 1:600, 1:300, 1:100, and 1:50, which were denoted as Ti-WACF, Mn/600Ti-N-WACF, Mn/300Ti-N-WACF, Mn/100Ti-N-WACF, Mn/50Ti-N-WACF, respectively.

2.2. Measurements

The surface morphology of the photocatalysts was observed using a FEI NANOSEM 430 scanning electron microscope (SEM, FEI, Hillsboro, OR, America) with thermal field emission.

The XRD diffractograms were obtained using a Rigaku D/max2500 powder X-ray diffractometer (Rigaku, Tokyo, Japan) installed with Cu Kα ray (λ = 1.5405 Å) and operated at the tube voltage of 40 kV, tube current of 100 mA, in the scanning angle (2θ) ranging from 20 to 80°, and scanning speed of 8° min^{-1}. The average diameter D (nm) of the photocatalysts were calculated using Scherrer formula $D = 0.89\lambda/(\beta\cos\theta)$, where λ is the X-ray wavelength (0.154 nm), θ is the Bragg angle of diffraction peaks (°) and β is full width at half maximum (FWHM). The FWHM of each diffraction line was determined from the profile measured with a scanning rate of 1/2° (2θ) min^{-1}, which was calibrated by standard silicon powder for instrumental broadening.

XPS measurements were carried out on a Kratos Axis UltraDLD multi-technique X-ray photoelectron spectroscopy (Shimadzu, Kyoto, Japan) with a monochromated Al Kα X-ray source (hν = 1486.6 eV). XPS survey spectra were recorded with pass energy of 80 eV, and high resolution spectra with pass energy of 40 eV. For calibration purposes, the C 1s electron binding energy corresponding to graphitic carbon was set at 284.6 eV. Atomic ratios were calculated from the XPS spectra after correcting the relative peak areas by sensitivity factors according to the transmission characteristics of the Physical Electronics SCA. A nonlinear least squares curve-fitting program (XPSPEAK software, Version 4.1) was used for XPS spectral deconvolution.

A UV-3600 spectrophotometer (Shimadzu, Kyoto, Japan) was used to characterize the UV-vis absorbance of the samples. The diffuse reflectance spectra of the samples over a range of 200–800 nm were recorded at room temperature in air from 200 to 700 nm.

The degradation of the model dyes (MB) was performed in a 200 mL reactor. A 65 W tungsten halogen lamp with a 400 nm cutoff filter was used as visible light source. The distance between the strip lamp and fluid level was kept at 15 cm. The initial concentration of the MB solution was 33 mg/L. Ten milligrams Mn/Ti-N-WACF and 100 mL of the MB aqueous solution were added into the reaction system. Before illumination, the suspension was magnetically stirred for 40 min in the dark to ensure that the mixture reached to the adsorption equilibrium. During the photoreaction process, 3 mL of the solution was collected periodically. The photocatalyst was separated from the solution by centrifugation, and the concentration of the remaining clear liquid was determined using UV-vis spectroscopy.

3. Results and Discussion

3.1. SEM Analysis

Figure 1 shows the SEM images of WACF and Mn/Ti-N-WACF. Compared with the original WACF (Figure 1a,b), the surface of Mn/Ti-N-WACF was covered with a uniform layer of Mn/N-co-doped nano-TiO_2 film (Figure 1c–h). The Mn/N-co-doped nano-TiO_2 was successfully loaded on the WACF surfaces; whereas the edges tilted in some regions, while some films peeled off from the WACF support. This might be attributed to the contraction of the base material and film during calcination. Mn/N-co-doped nano-TiO_2 showed mild agglomeration on the fiber surface. However, the agglomeration degree was less than that of the Mn/N-co-doped nano-TiO_2 powder. This finding indicates that a considerable number of pores on the WACF surface can help prevent the agglomeration of the nano-TiO_2 particles during the loading process. However, some parts of WACF base material were not covered completely after loading. Abundant pores on the non-loaded WACF surfaces could be favored for the subsequent UV-vis adsorption and photocatalytic functions.

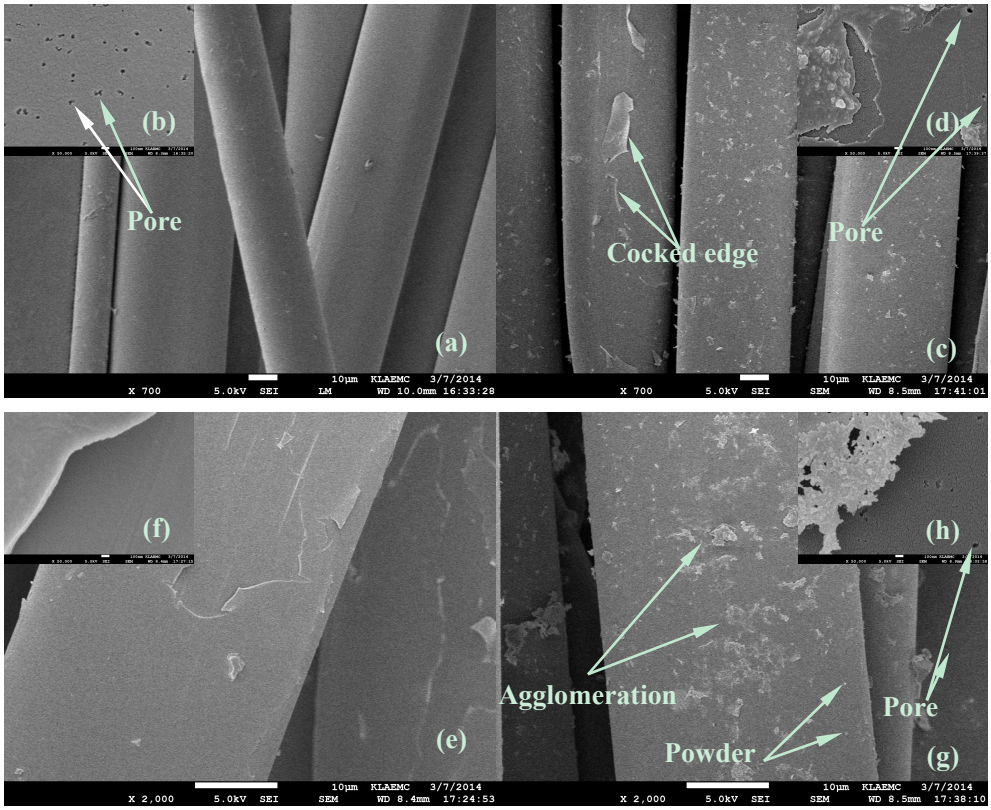

Figure 1. SEM images of activated carbon fibers from woody biomass (WACF) before (**a** and **b**) and after (**c**–**h**) loading of Mn/N-co-doped TiO_2. The inset micrographs (**b**, **d**, **f**, and **h**) were enlarged images.

3.2. XRD Analysis

The XRD patterns of activated carbon fiber loaded with Mn/N-co-doped TiO_2 after calcination at 450 °C are shown in Figure 2. All diffraction peaks of (101), (004), (200), (105), (211), (204), (220), and (215) correspond to the characteristic peaks of anatase TiO_2 [29–31]. No diffraction peaks of rutile

and brookite were found. This result indicated that under calcination at 450 °C, the Mn/N co-doping and loading on the activated carbon fiber did not affect the crystal phase of nano-TiO_2. As the Mn doping content increased, the peak of (101) for the co-doped samples shifted towards the left compared with pure TiO_2. The diffraction angle was decreased, and the interplanar spacing was increased. This phenomenon is contributed to the Mn/N doping in the TiO_2 lattice enhanced by the distortion of the octahedron in tetragonal anatase TiO_2. As the Mn doping content increased, the intensity of the peak was initially decreased and then increased. Only the sample Mn/50Ti-N-WACF showed higher intensity of peak (101) than that of pure TiO_2. This result indicated that Mn/N co-doping reduced the crystallization degree of TiO_2 when Mn/Ti ratio was <1/50. No impurity peaks related to Mn and N were found in the XRD patterns due to the low doping content.

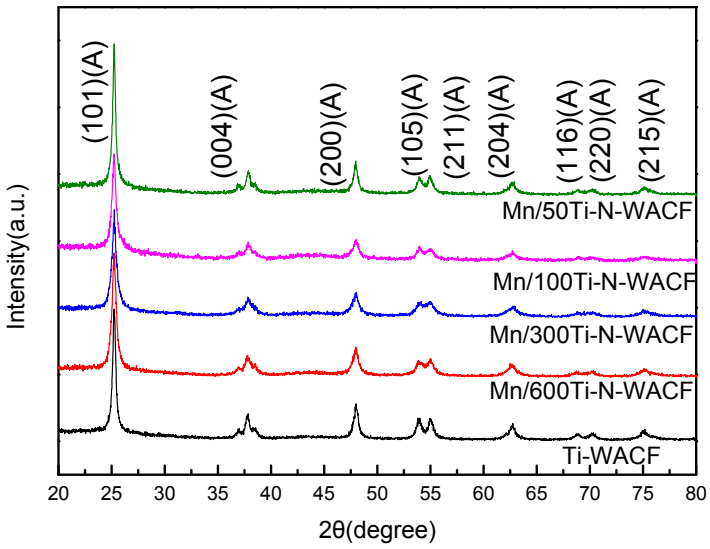

Figure 2. X-ray diffraction (XRD) patterns corresponding to different Mn doping contents.

Table 1 shows the mean grain diameters of the Mn/N-co-doped TiO_2 in the composite calculated using the Scherrer equation and the parameters of the peak (101). The mean grain diameters were within 23–37 nm, which ranges in the nano scale. All grain diameters of the Mn/N-co-doped TiO_2 were smaller than that of pure TiO_2. This indicated that Mn/N co-doping could effectively prevent the nano TiO_2 agglomeration during the calcination process. As the Mn doping content increased, the grain diameter in the composite was initially reduced to 26.6 nm for Mn/100Ti-N-WACF compared to pure TiO_2 (36.4 nm), and then increased to 36.2 nm for sample Mn/50Ti-N-WACF. Excess of Mn doping would cause the agglomeration of nano TiO_2 particles.

Table 1. Mean grain diameters of Mn/N-co-doped nano-TiO_2 in composites.

Sample	Ti-WACF	Mn/600Ti-N-WACF	Mn/300Ti-N-WACF	Mn/100Ti-N-WACF	Mn/50Ti-N-WACF
$2\theta_{101}$ (°)	25.24	25.23	25.24	25.22	25.23
β_{101} (°)	0.4325	0.5873	0.6739	0.5903	0.4344
Diameter (nm)	36.4	26.8	23.3	26.6	36.2

3.3. XPS Analysis

To obtain information about the chemical composition of the fiber surface and the binding characteristics of the elements at the surface, XPS measurements were carried out. The broad scan XPS spectra results of all samples were shown in Table 2. The range of 100–800 eV binding energies included the peaks of C 1s, O 1s, Ti 2p, Mn 2p, N 1s, and P 2p. This suggested that the samples were composed of the elements C, O, and Ti, as well as a small amount of Mn, N, and P. P was originated from the phosphoric acid added during phosphoric acid activation to prepare the liquefied wood. C (atom %) and O (atom %) were the dominant components, while the N content did not show any significant variation among all the composites samples but showed an opposite trend compared with the O content. The Ti content of Mn/Ti-N-WACF was higher than that of Ti-WACF. This was ascribed to the higher loading efficiency of Mn/N-co-doped TiO_2 on the porous surfaces of activated carbon fibers. The Ti content decreased as the Mn doping amount was increased. This phenomenon was probably caused by the substitution of the Ti ions by Mn ions in the TiO_2 lattice. Moreover, among all the co-doped samples Mn/300Ti-N-WACF had the highest O/C ratio.

Table 2. Global surface composition determined using X-ray photoelectron spectroscopies (XPS).

Samples	C		O		Ti		Mn		N		P		O/C
	BE (eV)	atom %	BE (eV)	atom %	BE (eV)	atom %	BE (eV)	atom %	BE (eV)	atom %	BE (eV)	atom %	(%)
Ti-WACF	284.5	73.18	531.6	25.87	458.8	0.91	636.8	0	401.1	0	135.0	0.04	35
Mn/600Ti-N-WACF	284.4	77.86	532.1	16.12	458.8	5.15	639.5	0.14	399.2	0.65	134.0	0.08	21
Mn/300Ti-N-WACF	284.4	74.80	531.9	20.71	458.7	3.64	640.1	0.15	398.9	0.56	131.9	0.14	28
Mn/100Ti-N-WACF	284.5	77.69	531.9	19.03	458.6	2.45	639.0	0.16	399.2	0.60	130.6	0.07	24
Mn/50Ti-N-WACF	484.5	77.46	532.1	17.90	458.6	3.69	641.1	0.19	399.1	0.62	128.7	0.14	23

Figure 3 shows the high-resolution XPS patterns of the Ti 2p orbital of the samples. The figure shows that the Ti 2p had two different orbitals, including Ti $2p_{1/2}$ (464.5 eV) and Ti $2p_{3/2}$ (458.8 eV). The energy interval between the two peaks was 5.7 eV, indicating that Ti existed in the form of Ti^{4+} in the samples [32]. As the Mn doping content increased, the Ti $2p_{3/2}$ binding energy shifted towards the lower energy and hybridization, which suggested that the electron density of the chemical environment surrounding Ti was increased due to partial O atoms was replaced by a few N atoms in the TiO_2 lattice.

For the N 1s orbital with increasing Mn doping content, the N 1s peaks of Mn/Ti-N-WACF appeared at 400.1, 399.7, 399.4, and 399.9 eV, for the samples of Mn/600Ti-N-WACF, Mn/300Ti-N-WACF, Mn/100Ti-N-WACF, and Mn/50Ti-N-WACF, respectively. To be noted that the range of 397.5 to 400.3 eV was corresponding to Ti–N–O. After the peak splitting of N 1s (Figure 4), the peaks also appeared in the regions of $\leqslant$397.5 eV (N–Ti–N) and $\geqslant$404 eV ascribing to NO_x [33,34]. This further confirmed that N of the Mn/Ti-N-WACF samples substituted some of the O atoms in the TiO_2 lattice.

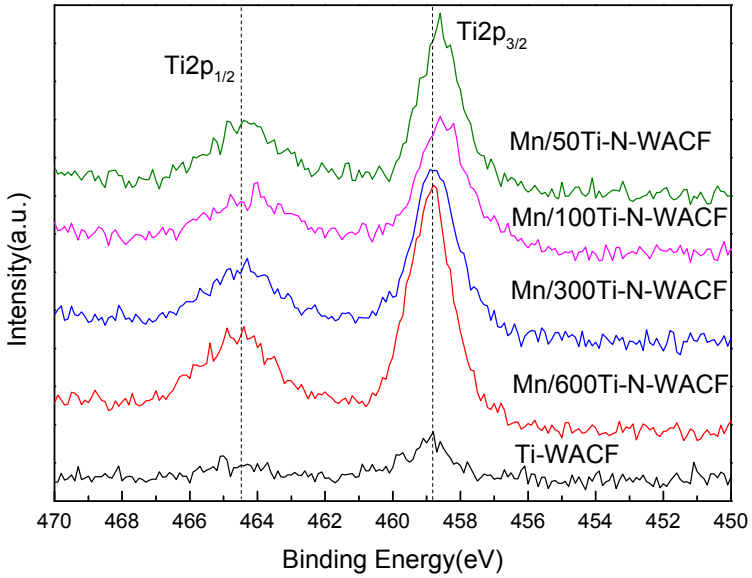

Figure 3. High-resolution Ti 2p XPS spectra of all samples.

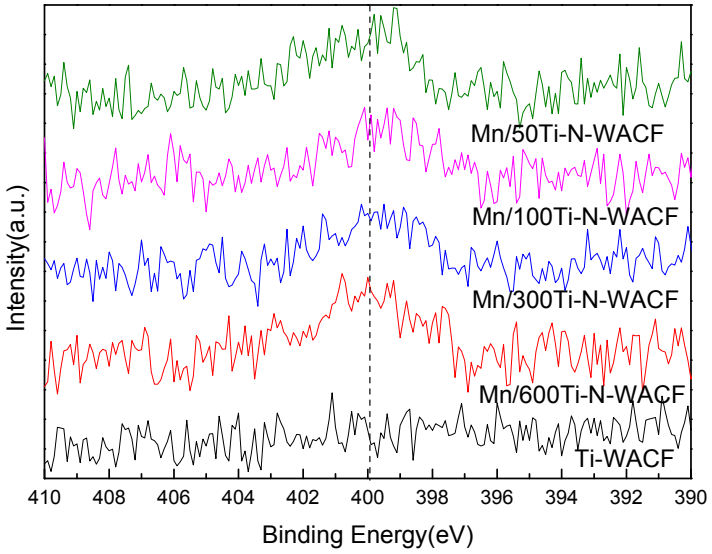

Figure 4. XPS spectra of various samples at the N 1s region.

The high-resolution C 1s spectra of the samples are shown in Figure 5. Deconvolution of the XPS C 1s spectra revealed five individual peaks that represent the following: graphitic carbon (C_{p1}, 284.6 eV); carbons present in phenol, alcohol, ether, or C=N groups (C_{p2}, 285.7–285.9 eV); carbonyl or quinine groups (C_{p3}, 286.4–287.0 eV); carboxyl, lactone, or ester groups (C_{p4}, 288.5–288.9 eV); and carbonate groups (C_{p5}, 289.5–290.8 eV) [35]. The percentages of carbon atoms from graphite or from different functional groups were calculated (Table 3). The intensity (mass %) of both graphitic carbon (C_{p1}) and carbons (C_{p2}–C_{p5}) in the oxygen-containing groups showed significant differences between Ti-WACF and Mn/Ti-N-WACF. The C_{p1} contents of all Mn/Ti-N-WACF samples were lower than that of Ti-WACF. In contrast, the C_{p3} contents of all Mn/Ti-N-WACF samples were higher than that of Ti-WACF. The emitted O from the TiO_2 colloids and the small amount of O substituted by N in the co-doped samples were absorbed by the pores present within activated carbon fiber during high-temperature calcination. Thus, the result indicated that Mn/N co-doping not only influenced the

TiO_2 lattice, but also indirectly affected the lattice composition of WACF. Compared with Ti-WACF, the Mn/N-co-doped samples contained C_{p5}, indicating that the co-doped samples had higher reactivity than Ti-WACF.

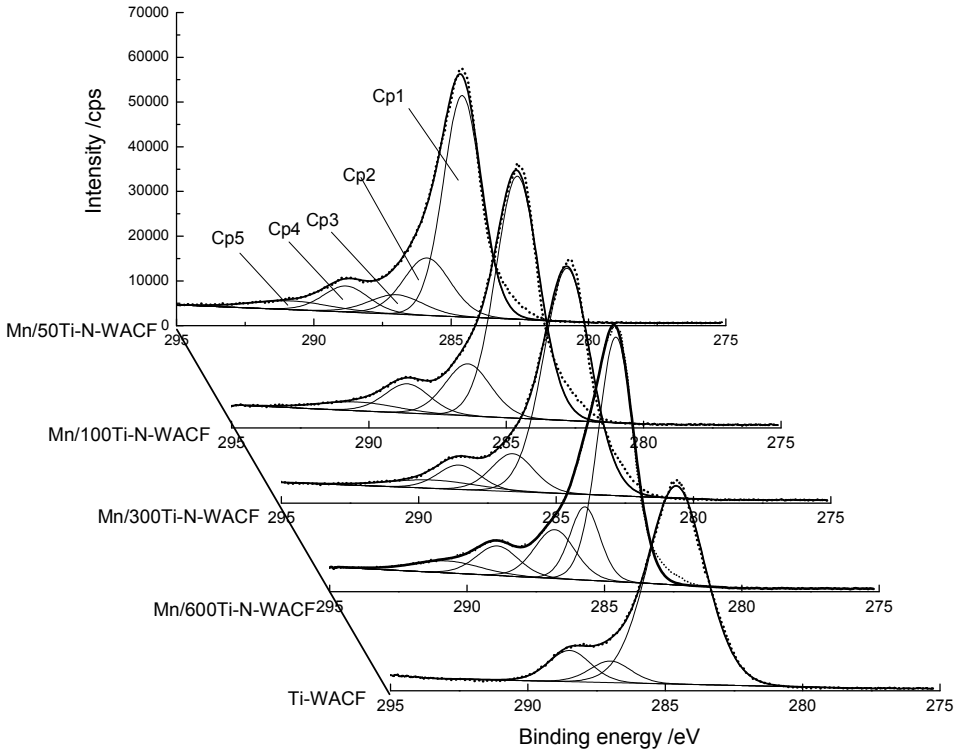

Figure 5. High-resolution fitted C 1s spectra of all samples.

Table 3. Results of fits of the C 1s regions. Values given as % of total intensity.

Samples	Graphite (C_{p1})		C–OH (C_{p2})		C=O (C_{p3})		C–OOH (C_{p4})		CO_3^{2-},CO.CO_2 (C_{p5})	
	BE (eV)	M (%)	BE (eV)	M (%)	BE (eV)	M (%)	BE (eV)	M (%)	BE (eV)	M (%)
Ti-WACF	284.6	83.9	-	-	287.0	6.5	288.5	9.6	-	-
Mn/600Ti-N-WACF	284.6	58.4	285.7	14.8	286.8	13.2	288.9	8.3	290.7	5.5
Mn/300Ti-N-WACF	284.6	76.0	-	-	286.6	11.4	288.5	7.4	289.5	5.2
Mn/100Ti-N-WACF	284.6	70.5	-	-	286.4	15.9	288.6	8.9	290.4	4.7
Mn/50Ti-N-WACF	284.6	60.0	285.9	19.2	287.0	7.4	288.8	8.4	290.8	4.9

Peak fitting of O 1s region of XPS spectra was conducted (Figure 6). Three individual peaks appeared at 530, 532, and 533.3 eV, were assigned to O_L (lattice oxygen), O_{OH} (hydroxyl oxygen), and O_{ad} (adsorbed oxygen), respectively [36,37]. Quantified area percentages of each peak are shown in Table 4. As the Mn doping content increased, The O_L contents of the Mn/Ti-N-WACF samples firstly increased and decreased. In contrast, the O_{OH} contents firstly decreased and increased. The O_{ad} contents of the co-doped samples increased with the Mn doping content increasing. Meanwhile, it was also obtained at 536 eV corresponding to the Ti–O–N bonds in Mn/Ti-N-WACF samples [28]. These findings were probably caused by the reaction of the doped N with O_{ad} forming NO_x during the high-temperature (450 °C) calcination process. Moreover, the O_L content of Mn/300Ti-N-WACF was significantly

higher than that of the other samples, indicating that this sample had good redox ability (*i.e.*, strong photocatalytic activity).

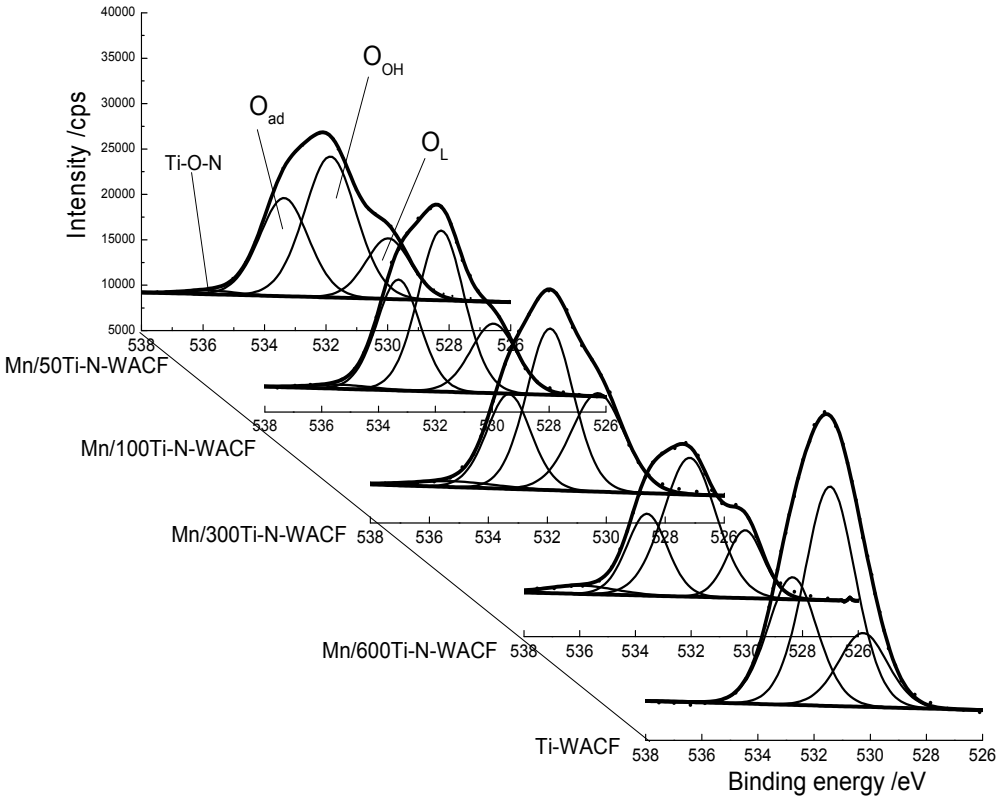

Figure 6. High-resolution fitted O 1s spectra of all samples.

Table 4. Results of fits of the O 1s regions. Values given as % of total intensity.

Samples	O_L		O_{OH}		O_{ad}		Ti–O–N	
	BE (eV)	M (%)	BE (eV)	M (%)	BE (eV)	M (%)	BE (eV)	M (%)
Ti-WACF	530.4	17.2	531.5	52.5	532.8	30.3	-	-
Mn/600Ti-N-WACF	530.0	18.0	532.1	53.7	533.6	24.1	535.9	4.2
Mn/300Ti-N-WACF	530.3	29.7	531.9	43.5	533.3	24.0	535.2	2.8
Mn/100Ti-N-WACF	529.8	20.4	531.8	47.3	533.3	30.7	535.4	1.6
Mn/50Ti-N-WACF	530.0	18.1	531.8	48.7	533.3	32.0	535.8	1.2

3.4. UV-vis Spectrometry

The UV-vis diffuse reflectance spectroscopy of Ti-WACF and Mn/Ti-N-WACF samples were shown in Figure 7. Compared with Ti-WACF, the absorption edge of the Mn/Ti-N-WACF samples shifted to the visible light region upon doping owing to the small amount of Mn that injected into the TiO_2 lattice or existed in the gap of TiO_2. It was further demonstrated that the Mn doping could narrow the band gap of TiO_2 and extend the absorption range of TiO_2 to visible light region. Moreover, Mn/Ti-N-WACF samples showed stronger visible light absorptions than Ti-WACF. The relatively strong absorption at 400–600 nm was attributed to the co-doping of N and Mn elements into the lattice of TiO_2 [38], and the chemical bonds of Ti–O–C rendered a red shift in the photo responding range and facilitated a more

efficient utilization of light for the photocatalysis [39,40]. With the Mn doping content was increased, the visible light absorbance of the Mn/Ti-N-WACF samples was initially increased and then decreased. This indicated that the higher Mn doping content significantly reduced the light absorption ability of the samples. It is also found that the light absorption of Mn/300Ti-N-WACF was the highest. The bandgap widths of the samples were calculated using the equation $E_g = 1240/\lambda_0$ (E_g is the bandgap width, and λ_0 is the threshold wavelength absorbed by the semiconductor) [41]. The bandgap widths of the Mn/Ti-N-WACF samples were slightly smaller than that of Ti-WACF. It was generally accepted that N doping could form an isolated N 2p narrow band above the O 2p valence band of TiO_2, which could decrease the band gap of TiO_2 and absorb visible light [42].

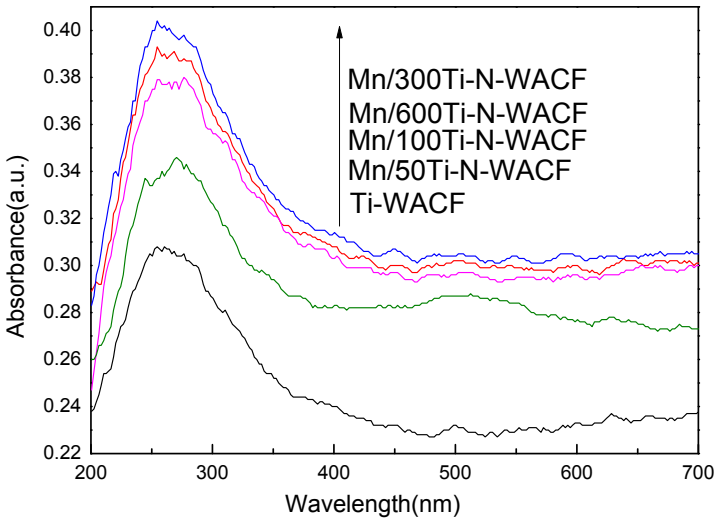

Figure 7. Ultraviolet–visible (UV-vis) absorption spectra of samples.

3.5. Photocatalytic Degradation of Methylene Blue

Figure 8 shows the photodegradation of methylene blue of all samples. With increasing lighting time, the degradation rates of methylene blue of all samples increased. After 60 min, the Mn/Ti-N-WACF-series had a higher degradation rate for methylene blue than Ti-WACF. After 240 min, the degradation rates for 33 mg/L methylene blue of the Mn/Ti-N-WACF-series reached 39%, 24%, 89%, and 93%. The degradation rate of methylene blue was indirectly proportional to the Mn doping content of the Mn/Ti-N-WACF-series. This result suggested that photocatalytic degradation is not only determined by the visible light absorption performance, but also by other factors, such as the electron-hole recombination rate and loading amount. It was also found that all of the Mn/Ti-N-WACF-series show enhanced photocatalytic degradation of MB as compared to the commercial P25 [43], and the photocatalytic degradation of Mn/50Ti-N-WACF samples for MB still reached up to 90% after the same experiment was carried out 3 times. Moreover, all the Mn/Ti-N-WACF-series samples showed significant visible light responsive activities for the degradation of MB compared to TiO_2 powder, owing to WACF being their carrier.

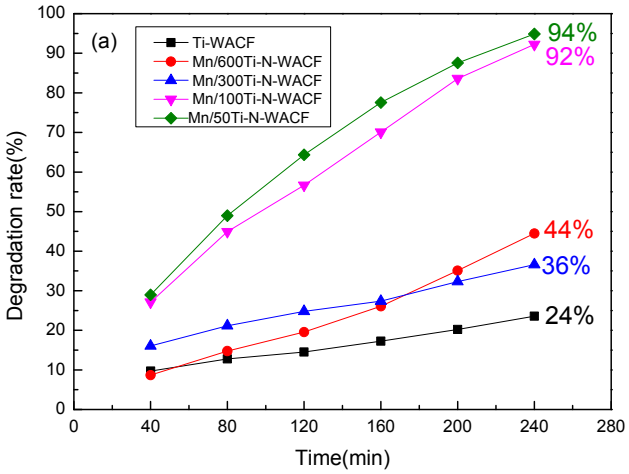

Figure 8. Photodegradation under visible light of methylene blue (MB) of all samples.

4. Conclusions

Mn/N co-doped TiO_2 loaded on wood-based activated carbon fiber (Mn/Ti-N-WACF) were successfully prepared by sol–gel and impregnation method. Mn/N co-doping could improve the loading rate of TiO_2 on the Mn/Ti-N-WACF surface. With increasing Mn doping content, the TiO_2 diameter of Mn/Ti-N-WACF was initially decreased and then increased. The Ti content of Mn/Ti-N-WACF was higher than that of Ti-WACF, and decreased with increasing Mn doping content. In addition, N in the Mn/Ti-N-WACF samples substituted some of the O atoms in the TiO_2 lattice. The bandgap width of the Mn/Ti-N-WACF samples was slightly smaller than that of Ti-WACF because of the Mn/N co-doping. This stimulated the photocatalytic activity of the Mn/Ti-N-WACF samples for methylene blue degradation under visible-light irradiation.

Acknowledgments

This research was financially supported by National Natural Science Foundation of China (No. 31270607).

Author Contributions

Yin Chen performed most of the experimental work and materials measurements. Xiaojun Ma contributed to the analysis of the results and to the writing of the manuscript.

Conflicts of Interest

The authors declare no conflict of interest.

References

1. Linsebigler, A.L.; Lu, G.Q.; Yates, J.T. Photocatalysis on TiO_2 surfaces: Principles, mechanisms, and selected results. *Chem. Rev.* **1995**, *95*, 735–758. [CrossRef]

2. Mills, A.; Elliott, N.; Hill, G.; Fallis, D.; Durrant, J.R.; Willis, R.L. Preparation and characterisation of novel thick sol–gel titania film photocatalysts. *Photochem. Photobiol. Sci.* **2003**, *2*, 591–596. [CrossRef] [PubMed]
3. Kudo, A.; Omori, K.; Kato, H. A novel aqueous process for preparation of crystal form-controlled and highly crystalline $BiVO_4$ powder from layered vanadates at room temperature and its photocatalytic and photophysical properties. *J. Am. Chem. Soc.* **1999**, *121*, 11459–11467. [CrossRef]
4. Anpo, M.; Takeuchi, M. The design and development of highly reactive titanium oxide photocatalysts operating under visible light irradiation. *J. Catal.* **2003**, *216*, 505–516. [CrossRef]
5. Zhao, L.; Yu, Y.; Song, L.; Hu, X.; Larbot, A. Synthesis and characterization of nanostructured titania film for photocatalysis. *Appl. Surf. Sci.* **2005**, *239*, 285–291. [CrossRef]
6. Chen, X.; Burda, C. The electronic origin of the visible-light absorption properties of C-, N- and S-doped TiO_2 nanomaterials. *J. Am. Chem. Soc.* **2008**, *130*, 5018–5019. [CrossRef] [PubMed]
7. Dong, M.J.; In, H.K.; El, L.K.; Chan, S.J.; Hyung, S.L.; Kidong, P.; Jeunghee, P. Transition-Metal doping of oxide nanocrystals for enhanced catalytic oxygen evolution. *J. Phys. Chem. C* **2015**, *119*, 1921–1927.
8. Vinodgopal, K.; Ulick, S.; Kimberly, A.G.; Prashant, V.K. Eletrochemically assisted photocatalysis. 2. The role of oxygen and reaction intermediates in the degradation of 4-chlorophenol on immobilized TiO_2 particulate films. *J. Phys. Chem.* **1994**, *98*, 6797–6803. [CrossRef]
9. Klosek, S.; Raftery, D. Visible light driven V-doped TiO_2 photocatalyst and its photooxidation of ethanol. *J. Phys. Chem. B* **2001**, *105*, 2815–2819. [CrossRef]
10. Paola, A.D.; Marcì, G.; Palmisano, L.; Schiavello, M.; Uosaki, K.; Ikeda, S.; Ohtani, B. Preparation of polycrystalline TiO_2 photocatalysts impregnated with various transition metal ions: Characterization and photocatalytic activity for the degradation of 4-nitrophenol. *J. Phys. Chem. B* **2002**, *106*, 637–645. [CrossRef]
11. Zhu, J.; Zheng, W.; He, B.; Zhang, J.; Anpo, M. Characterization of Fe–TiO_2 photocatalysts synthesized by hydrothermal method and their photocatalytic reactivity for photodegradation of XRG dye diluted in water. *J. Mol. Catal. A: Chem.* **2004**, *216*, 35–43. [CrossRef]
12. Fei, D.Q.; Hudaya, T.; Adesina, A.A. Visible-light activated titania perovskite photocatalysts: Characterisation and initial activity studies. *Catal. Commun.* **2005**, *6*, 253–258. [CrossRef]
13. Binas, V.D.; Sambani, K.; Maggos, T.; Katsanaki, A.; Kiriakidis, G. Synthesis and photocatalytic activity of Mn-doped TiO_2 nanostructured powders under UV and visible light. *Appl. Catal. B Environ.* **2012**, *113*, 79–86. [CrossRef]
14. Sambrano, J.R.; Nobrega, G.F.; Taft, C.A.; Andres, J.; Beltran, A. A theoretical analysis of the TiO_2/Sn doped (110) surface properties. *Surf. Sci.* **2005**, *580*, 71–79. [CrossRef]
15. Choi, J.; Park, H.; Hoffmann, M.R. Effects of single metal-ion doping on the visible-light photoreactivity of TiO_2. *J. Phys. Chem. C* **2010**, *114*, 783–792. [CrossRef]
16. Kim, J.; Choi, W. TiO_2 modified with both phosphate and platinum and its photocatalytic activities. *Appl. Catal. B Environ.* **2011**, *106*, 39–45. [CrossRef]

17. Di, L.; Zhang, X.; Xu, Z.; Wang, K. Atmospheric-pressure cold plasma for preparation of high performance Pt/TiO_2 photocatalyst and its mechanism. *Plasma Chem. Plasma Process.* **2014**, *34*, 301–311. [CrossRef]
18. Magagnin, L.; Bernasconi, R.; Ieffa, S.; Diamanti, M.V.; Pezzoli, D.; Candiani, G.; Pedeferri, M.P. Photocatalytic and antimicrobial coatings by electrodeposition of silver/TiO_2 nano-composites. *ECS Trans.* **2013**, *45*, 1–6. [CrossRef]
19. Ruggieri, F.; di Camillo, D.; Maccarone, L.; Santucci, S.; Lozzi, L. Electrospun Cu-, W- and Fe-doped TiO_2 nanofibres for photocatalytic degradation of rhodamine 6G. *J. Nanopart. Res.* **2013**, *15*, 1982–1992. [CrossRef]
20. Asahi, R.; Morikawa, T.; Ohwaki, T.; Aoki, K.; Taga, Y. Visible-light photocatalysis in nitrogen-doped titanium oxides. *Science* **2001**, *293*, 269–271. [CrossRef] [PubMed]
21. Aditi, R.G.; Julio, B.F. A simple method to synthesize N-doped rutile titania with enhanced photocatalytic activity in sunlight. *J. Solid State Chem.* **2005**, *178*, 2953–2957.
22. Liu, S.; Syu, H. One-step fabrication of N-doped mesoporous TiO_2 nanoparticles by self-assembly for photocatalytic water splitting under visible light. *Appl. Energ.* **2012**, *100*, 148–154. [CrossRef]
23. Jaiswal, R.; Bharambe, J.; Patel, N.; Dashora, A.; Kothari, D.C.; Miotello, A. Copper and Nitrogen co-doped TiO_2 photocatalyst with enhanced optical absorption and catalytic activity. *Appl. Catal. B Environ.* **2015**, *168*, 333–341. [CrossRef]
24. Liu, J.H.; Yang, R.; Li, S.M. Preparation and application of efficient TiO_2/ACFs photocatalyst. *J. Environ. Sci.* **2006**, *18*, 979–982. [CrossRef]
25. Yao, S.H.; Li, J.Y.; Shi, Z.L. Immobilization of TiO_2 nanoparticles on activated carbon fiber and its photodegradation performance for organic pollutants. *Particuology* **2010**, *8*, 272–278. [CrossRef]
26. Ma, X.; Zhao, G. Preparation of carbon fibers from liquefied wood. *Wood Sci. Technol.* **2010**, *44*, 3–11.
27. Ma, X.; Zhang, F.; Zhu, J.; Yu, L.; Liu, X. Preparation of highly developed mesoporous activated carbon fiber from liquefied wood using wood charcoal as additive and its adsorption of methylene blue from solution. *Bioresour. Technol.* **2014**, *164*, 1–6. [CrossRef] [PubMed]
28. Li, D.; Ma, X. Preparation and characterization of activated carbon fibers from liquefied wood. *Cellulose* **2013**, *20*, 1649–1656. [CrossRef]
29. Wonyong, C.; Andreas, T.; Michael, R.H. The role of metal ion dopants in quantum-sized TiO_2: Correlation between photoreactivity and charge carrier recombination dynamics. *J. Phys. Chem.* **1994**, *98*, 13669–13679.
30. Marci, G.; Palmisano, L.; Sclafani, A.; Venezia, M.; Campostrini, R.; Carturan, G.; Martin, C.; Rives, V.; Solana, G. Influence of tungsten oxide on structural and surface properties of sol–gel prepared TiO_2 employed for 4-nitrophenol photodegradation. *J. Chem. Soc. Faraday Trans.* **1996**, *92*, 819–829. [CrossRef]
31. Navio, J.A.; Colon, G.; Macias, M.; Real, C.; Litter, M.I. Iron-doped titania powders prepared by a sol–gel method: Part II: Photocatalytic properties. *Appl. Catal. A Gen.* **1999**, *178*, 191–203. [CrossRef]
32. Bourgeois, S.; Le, S.P.; Perdereau, M. Study by XPS of ultra-thin nickel deposits on TiO_2 (100) supports with different stoichiometries. *Surf. Sci.* **1995**, *328*, 105–110. [CrossRef]

33. Chauhan, R.; Kumar, A.; Chaudhary, R.P. Structural and photocatalytic studies of Mn doped TiO_2 nanoparticles. *Spectrochim Acta Part A Mol. Biomol. Spectrosc.* **2012**, *98*, 256–264. [CrossRef] [PubMed]
34. Yang, G.D.; Jiang, Z.; Shi, H.H.; Xiao, T.; Yan, Z. Preparation of highly visible-light active N-doped TiO_2 photocatalst. *J. Mater. Chem.* **2010**, *20*, 5301–5309. [CrossRef]
35. Chiang, Y.C.; Lee, C.Y.; Lee, H.C. Surface chemistry of polyacrylonitrile- and rayon-based activated carbon fibers after post-heat treatment. *Mater. Chem. Phys.* **2007**, *101*, 199–210. [CrossRef]
36. Inagaki, M.; Hirose, Y.; Matsunaga, T.; Tsumura, T.; Toyoda, M. Carbon coatings of anatase-type TiO_2 through their precipitation in PVA aqueous solution. *Carbon* **2003**, *41*, 2619–2624. [CrossRef]
37. Rincon, M.E.; Trujillo-Camacho, M.E.; Cuentas-Gallegos, A.K.; Casillas, N. Surface characterization of nanostructured TiO_2 and carbon blacks composites by dye adsorption and photoelectrochemical studies. *Appl. Catal. B Environ.* **2006**, *69*, 65–74. [CrossRef]
38. Zou, X.X.; Li, G.D.; Guo, M.Y.; Li, X.H.; Liu, D.P.; Su, J.; Chen, J.S. Heterometal alkoxidesas precursors for the preparation of porous Fe- and Mn-TiO_2 photocatalystswith high efficiencies. *Chem. Eur. J.* **2008**, *14*, 11123–11131. [CrossRef] [PubMed]
39. Liu, S.; Sun, H.; Liu, S.; Wang, S. Graphene facilitated visible light photodegradation of methylene blue over titanium dioxide photocatalysts. *Chem. Eng. J.* **2013**, *214*, 298–303. [CrossRef]
40. Yao, Y.; Li, G.; Ciston, S.; Lueptow, R.M.; Gray, K.A. Photoreactive TiO_2/carbon nanotube composites: Synthesis and reactivity. *Environ. Sci. Technol.* **2008**, *42*, 4952–4957. [CrossRef] [PubMed]
41. Huang, W.; Tang, X.; Wang, Y.; Koltypin, Y.; Gedanken, A. Selective synthesis of anatase and rutile via ultrasound irradiation. *Chem. Commun.* **2000**, *15*, 1415–1416. [CrossRef]
42. Irie, H.; Watanabe, Y.; Hashimoto, K. Nitrogen-concentration dependence on photocatalytic activity of $TiO_{2-x}N_x$ powders. *J. Phys. Chem. B* **2003**, *107*, 5483–5486. [CrossRef]
43. Li, J.; Zhou, S.L.; Hong, G.B.; Chang, C.T. Hydrothermal preparation of P25–graphene composite with enhanced adsorption and photocatalytic degradation of dyes. *Chem. Eng. J.* **2013**, *219*, 486–491. [CrossRef]